IEEE JOURNAL OF EMERGING AND SELECTED TOPICS IN INDUSTRIAL ELECTRONICS

Frequency-Adaptive Energy Control for Grid-Forming MMCs Under Unbalanced Conditions

Eros Avdiaj, Salvatore D'Arco, Luigi Piegari, *Senior Member, IEEE,* and Jon Are Suul, *Member, IEEE*

***Abstract* – This paper presents a frequency-adaptive energy control strategy for a Modular Multilevel Converter (MMC) which is suitable for grid-forming operation under unbalanced conditions. The average components of the energy sum and energy difference feedback signals for each phase are extracted by frequency-adaptive notch filters based on Second Order Generalized Integrators (SOGIs). Frequency-adaptivity is provided by utilizing the internal frequency defined by the power-balance-based synchronization mechanism of the grid-forming control. This approach prevents the filtering performance from degrading under islanded operation and other weak grid conditions where large frequency variations can occur. A comparative analysis between the frequency-adaptive notch filtering (FA-NF) and an implementation based on conventional fixed-width moving average filters (MAF) is presented. In addition to the improved performance at off-nominal frequency, the SOGI-based FA-NF implementation reduces the delay in the energy feedback signals compared to the MAF-based reference case, resulting in improved stability margins and a more damped response. The performance of the proposed energy control strategy is comprehensively demonstrated by time-domain simulations of an HVDC terminal and by experimental testing on a 50 kVA MMC prototype. Both grid connected and islanded conditions are evaluated while considering 5 different strategies for controlling the negative sequence currents during unbalanced conditions.**

***Index Terms*—Energy Control, Filtering, Frequency Adaptivity, Grid Forming Control, Modular Multilevel Converter, Unbalanced Grid Voltage, Virtual Synchronous Machines**

Manuscript received 21 December 2022; revised 28 April 2023 and 12 June 2023; accepted 20 July 2023. Date of publication xx August 2023; date of current version 30 July 2023. The manuscript is partly based on the paper "Adaptive Filtering for Energy Control of a Modular Multilevel Converter Operated as a Virtual Synchronous Machine Under Unbalanced Conditions, presented at the IEEE CPE-POWERENG, Birmingham, UK, 29 June – 1 July, 2022. The work was supported by the HVDC Inertia Provision (HVDC Pro) Project funded by the ENERGIX Program of the Research Council of Norway (RCN) under Grant 268053/E20, with industry partners Statnett, Equinor, RTE, and ELIA, and by the Ocean Grid Research Project, funded by the Green Platform instrument of the RCN under Grant 328750 *(Corresponding author: Jon Are Suul.)*

Eros B. Avdiaj and Luigi Piegari are with the Department of Electronics, Information and Bioengineering, Politecnico di Milano, 20133 Milan, Italy (e-mail: avdiaj.eros@gmail.com; luigi.piegari@polimi.it).

Salvatore D'Arco is with SINTEF Energy Research, 7465 Trondheim, Norway (e-mail: salvatore.darco@sintef.no)

Jon Are Suul is with SINTEF Energy Research, 7465 Trondheim, Norway, and also with the Department of Engineering Cybernetics, Norwegian University of Science and Technology, 7491 Trondheim, Norway (e-mail: jon.a.suul@sintef.no).

Color versions of one or more figures in this article are available at https://doi.org/xx.yyyy/JESTIE.2023....

Digital Object Identifier xx.yyyy/JESTIE.2023….

NOMENCLATURE

General Conventions

Upper case symbols represent quantities in the SI system
Lower case symbols represent per unit quantities
Bold fonts represent complex or space vector quantities

Main variables and parameters

V	Voltage
I	Current
P, Q	Active, Reactive power
W	Energy
R, L, C, X	Resistance, Inductance, Capacitance, Reactance
Ω	Angular frequency (in rad/s)
θ	Phase angle (in rad)
N	Number of sub-modules in an MMC arm
T_a	Inertia time constant of Virtual Synchronous Machine
k_d	Damping coefficient of Virtual Synchronous Machine

Symbol modifiers

$\hat{\square}$	Amplitude of three phase quantity or oscillating component
$\lvert\square\rvert$	Absolute value of complex vector quantities
$\bar{\square}$	Extracted average value or dc-component of a signal

Superscripts

$+,-$	Positive, Negative sequence component
dc	Average value or dc-component of a signal
ω	Fundamental frequency component
PI	Term resulting as output of a PI regulator
$*$	Reference value for control
Σ	Sum of quantities
Δ	Difference of quantities

Subscripts

C	Quantities associated with MMC equivalent arm capacitance
SM	Sub-module of MMC arm
T	Equivalent quantities associated with transformer
a, b, c, k	Phases a,b and c or unspecified phase k
u, l	Upper, Lower MMC arm quantities
b	Base value for per unit system
e	Equivalent voltage behind a virtual impedance
i	Integral term (of PI controller)
o	Output terminals at the PCC
p	Proportional gain (of PI controller)
v	Converter ac side quantities
cir	Circulating quantities of the internal MMC dynamics
g	Grid parameters
dc	Direct current component
dq	Synchronous reference frame direct and quadrature axis comp.
$\alpha\beta$	Stationary frame orthogonal components
w	Window width for MAF
z	Zero sequence component

Abbreviations

BPSC	Balanced Positive Sequence Currents
CAP	Constant Active Power flow
CCC	Circulating Current Controller
CCVSM	Current Controlled VSM
CRP	Constant Reactive Power flow
FA	Frequency Adaptive

FF	Fixed Frequency
MAF	Moving Average Filter
MMC	Modular Multilevel Converter
NF	Notch Filter
NSVC	Negative Sequence Voltage Control
NSVI	Negative Sequence Virtual Impedance
PCC	Point of Common Coupling
PIR	Proportional Integral Resonant
PLL	Phase Locked Loop
PR	Proportional Resonant
QSG	Quadrature Signal Generator
SM	Sub-Module (of MMC)
SOGI	Second Order Generalized Integrator
VI	Virtual Impedance
VSC	Voltage Source Converter
VSM	Virtual Synchronous Machine

I. INTRODUCTION

The concept of grid-forming control has been identified as important for the development of future transmission systems with a dominant presence of converter-interfaced generation [1]-[3]. Relevant candidates for providing grid-forming functionality include HVDC transmission systems based on modern Voltage Source Converter (VSC) topologies with high controllability and power capability. Specifically, the double-star Modular Multilevel Converter (MMC) topology has become the dominant solution in HVDC transmission systems for renewable power integration and weak grid conditions [4], [5]. Thus, the internal dynamics and energy balancing of the MMC should be studied together with the general challenges of the ac-side control when considering grid-forming HVDC converters.

Initial discussions and analysis on the role of the energy control in grid-forming operation of MMCs were presented in [6]-[8]. However, these studies did not consider the energy balancing control under unbalanced fault conditions. While also other previous publications have discussed the application of grid-forming control to MMCs, including the proposals of Virtual Synchronous Machine (VSM)-based control in [9]-[13], they have not explicitly examined the control under unbalanced conditions. Furthermore, none of these publications explored the impact of grid frequency variations on the MMC energy balancing control.

For conventional grid-following control, the energy balancing of MMCs during unbalanced conditions has been thoroughly studied, as reviewed in [14]. The first examples of extending such studies to grid-forming control strategies while considering unbalanced grid fault conditions have been presented in [15]-[17]. Still, these publications have only considered operation in grid-connected mode, while islanded operation or conditions with large frequency variations have not been studied. Thus, the energy control loops are usually based on fixed frequency notch filters or fixed-width moving average filters (MAF) for detecting the dc-component of the energy feedback signals. This also implies that the energy control loops of the MMC have been kept independent from the frequency dynamics of the grid-forming control.

A closed-loop MMC energy control strategy for grid forming operation under unbalance conditions, relying on explicitly frequency-adaptive filtering for detecting the dc-component of the energy sum and energy difference feedback signals, was first presented in [18]. The frequency-adaptivity of the feedback signal filtering was ensured by using the frequency from the virtual swing equation of a VSM-based control system as input to Second Order Generalized Integrator (SOGI)-based Quadrature Signal Generators (QSGs) configured as notch filters. The energy control strategy was presented in detail, and the importance of the frequency adaptive filtering for operation during grid frequency variations was demonstrated by time-domain simulations. However, [18] did not consider islanded operation and included only results obtained with a VSM-based ac-side control for imposing balanced currents during unbalanced voltages.

The energy control strategy presented in [18] was developed for MMCs by utilizing the VSM-based scheme from [19], [20]. In these previous works, it was demonstrated how different negative sequence current control strategies for handling unbalanced grid conditions can be integrated in a VSM-based control system. It was also assessed how these strategies perform under grid-connected and islanded operation. This paper extends the work in [18], by further analysis, simulations, and experiments. Thus, it is evaluated how the proposed frequency-adaptive notch-filtering can provide improved performances in terms of stability margins and transient response to disturbances, as well as improved steady-state energy control during large deviations from the nominal frequency. Together with [18], the main contributions of the presented work can be summarized as:

- Development of an MMC energy control strategy suitable for grid forming operation under unbalanced conditions and large frequency variations. The implementation is made inherently frequency adaptive by using the speed of the virtual swing equation in a VSM-based grid forming control as input to SOGI-based notch filters.
- Theoretical analysis and verification by time-domain simulations and experiments of how the proposed SOGI-based filtering in the energy feedback signal can provide improved stability margin and transient response of the energy control compared to a control implementation based on fixed-width MAFs.
- Comprehensive verification by time-domain simulations and laboratory experiments of how the proposed energy control strategy maintains the expected performance when applied together with the different strategies for ac-side negative sequence current control defined in [19], [20], considering both grid-connected and islanded operation. The results also demonstrate the advantage of frequency adaptivity in the MMC energy control when operating with large deviations from the nominal frequency.

It should be noted that the implementation of the overall grid forming control system is also relying on SOGI-based symmetrical sequence component detection and resonant current controllers which are made frequency-adaptive by the virtual speed of the VSM. To the best knowledge of the

Author Accepted Manuscript version of the article by Eros Avdiaj, Salvatore D'Arco and Jon Are Suul.
in IEEE Journal of Emerging and Selected Topics in Industrial Electronics, Vol 4 (2023) Page 1124-1137, DOI: http://dx.doi.org/10.1109/JESTIE.2023.3302707.

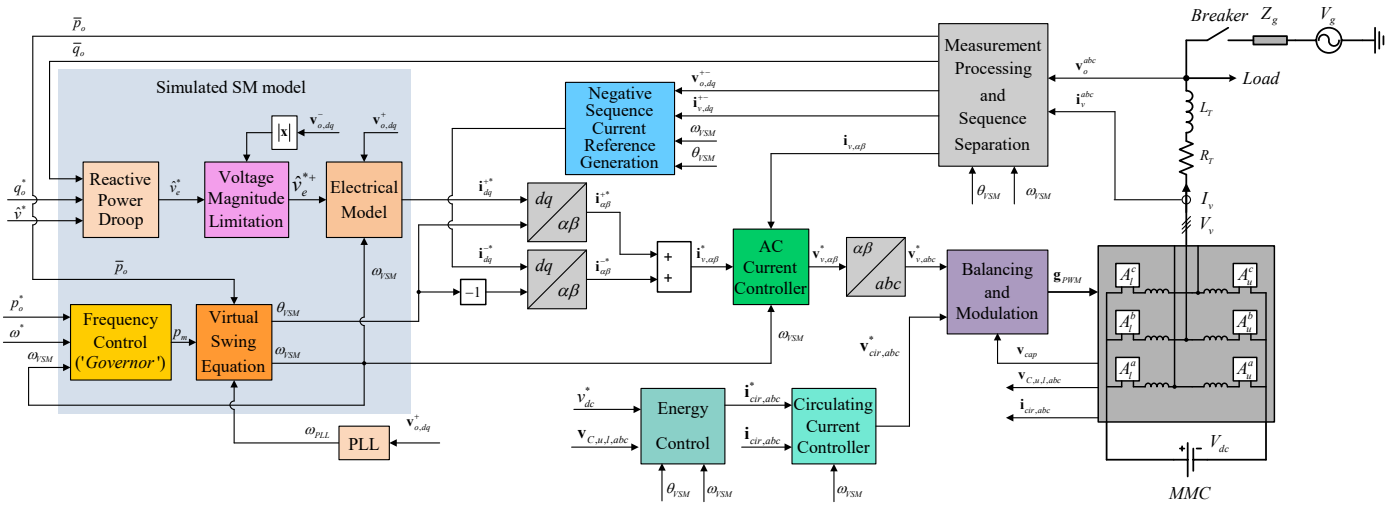

Fig. 1 Overview of VSM-based control strategy for operation under unbalanced conditions, adapted from [18] and [19].

authors, no similar comprehensive analysis of MMC energy control, that considers unbalanced operating conditions, VSM-based grid forming functionality, and operation with large frequency variations, are available in previous literature.

II. Overview of Studied VSM-based MMC Control for Operation Under Unbalanced Conditions

An overview of the studied VSM-based grid-forming control for an MMC from [18], with the main elements adapted from [19] and [20], is presented in Fig. 1. As indicated in the figure, the scheme is based on stationary frame current controllers for unbalanced operation without depending on positive and negative sequence decoupling in the inner loops. The implementation relies on SOGI-based Proportional-Resonant (PR) controllers, according to [21], where frequency-adaptivity is ensured by using the virtual speed of the VSM. The basic functions of the control system are briefly reviewed in the following, based on the detailed descriptions in [18]-[20], while the impact of the filtering approach in the energy control loops is discussed in detail in section III. In all discussions, upper case symbols are used for physical quantities, while lower case symbols denote per unit quantities.

A. Virtual swing equation

The grid-forming features of the VSM are mainly defined by the virtual swing equation intended to emulate the rotor dynamics of a synchronous machine. When including a power-frequency droop for representing the steady-state characteristics of the governor in a conventional generator, the virtual speed, ω_{VSM}, is defined by [22]:

$$T_a \frac{d\omega_{VSM}}{dt} = k_\omega \left(\omega^*_{VSM} - \omega_{VSM}\right) + k_d \left(\omega_{VSM} - \omega_{PLL}\right) + p^*_o - \bar{p}_o , \quad (1)$$

where T_a is the mechanical time constant and ω^*_{VSM} is the external frequency reference, while ω_{PLL} is the grid angular frequency as estimated by a Phase Locked Loop (PLL). The droop gain and the damping coefficient are defined by k_ω and k_d, respectively, while the active power set-point is given by p^*_o. The implementation of the VSM swing equation and of

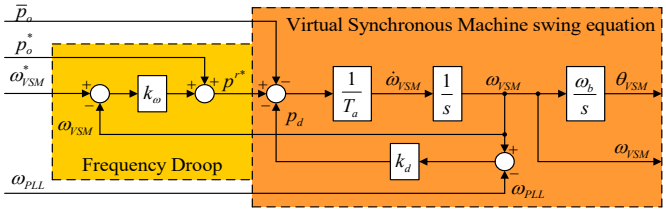

Fig. 2 Virtual swing equation of VSM for operation in unbalanced conditions

the frequency droop controller can be graphically represented by the scheme reported in Fig. 2.

The main adaptation of the basic VSM-swing equation from [22] for operation under unbalanced conditions is that the dc-component of the instantaneous active power flow, $\bar{p}_o$, is used as the feedback signal in (1) [19], [20]. Furthermore, the PLL for grid frequency detection operates on the positive sequence component of the measured voltage. The positive and negative sequence detection used for the PLL, as well as for the calculation of the average power flow, relies on the SOGI-QSG-based strategy from [23]. However, the frequency-adaptivity of the SOGI-QSGs utilizes the VSM speed instead of the frequency estimation from the PLL.

B. Reactive power droop and positive sequence current reference calculation

The positive sequence voltage reference for the VSM is provided by a simple reactive power droop as:

$$\hat{v}^{+*}_e = \hat{v}^* + k_q \left(q^*_o - \bar{q}_o\right), \quad (2)$$

where $\hat{v}_e{}^{+*}$ is the reference used for the internal control, while $\hat{v}^*$ is the external reference for the voltage amplitude, $q_o{}^*$ is the reactive power reference, $\bar{q}_o$ is the dc-component of the reactive power flow, and k_q is the reactive power droop coefficient [20]. As further explained in [20], the internal positive sequence voltage magnitude of the VSM is limited to:

$$0 < \hat{v}^{+*}_e < k_{v,\text{lim}} \cdot \left(1 - \left|\mathbf{v}^-_o\right|\right), \quad (3)$$

where $k_{v,\text{lim}}$ is the voltage limiting factor and $|\mathbf{v}_o{}^-|$ is the amplitude of the negative sequence voltage.

Author Accepted Manuscript version of the article by Eros Avdiaj, Salvatore D'Arco and Jon Are Suul.
in IEEE Journal of Emerging and Selected Topics in Industrial Electronics, Vol 4 (2023) Page 1124-1137, DOI: http://dx.doi.org/10.1109/JESTIE.2023.3302707.

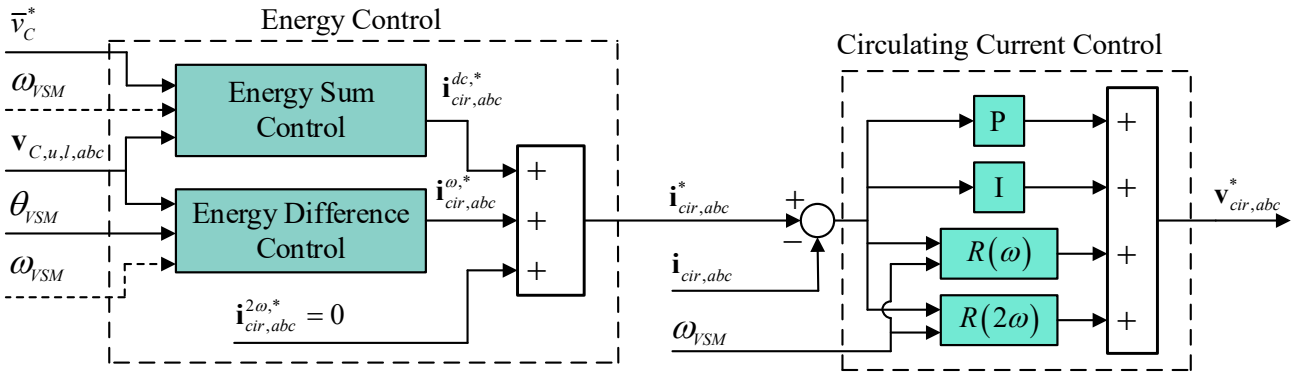

Fig. 3 Overview of MMC energy control and circulating current control [18]

The control strategies discussed in [19] and [20] are based on the Current Controlled VSM (CCVSM) concept from [24]. By considering separate control of the positive and negative sequence currents, the positive sequence current reference is calculated in the positive sequence synchronous reference frame as:

$$\mathbf{i}_v^{+,*}=\frac{\hat{v}_e^{+*}-\mathbf{v}_o^{+}}{r_{VI}^{+}+j\omega_{VSM}l_{VI}^{+}}. \tag{4}$$

Here, $\mathbf{v}_o^+$ is the measured positive sequence voltage, while r_{VI}^+ and l_{VI}^+ are the virtual resistance and inductance, respectively.

C. Negative sequence current reference calculation

In [19], [20], five different strategies were studied for negative sequence current control of a VSM under unbalanced conditions. Firstly, three options were defined for controlling the power flow characteristics to achieve either balanced positive sequence currents (BPSC), constant active power flow (CAP) or constant reactive power flow (CRP). These three control strategies can be unified in one expression as:

$$\mathbf{i}_v^{-*}=\begin{bmatrix} i_{v,d}^{-*} \\ i_{v,q}^{-*}\end{bmatrix}=\frac{k^-}{(v_{o,d}^+)^2+(v_{o,q}^+)^2} \cdot \begin{bmatrix} v_{o,d}^+v_{o,d}^- - v_{o,q}^+v_{o,q}^- & v_{o,q}^+v_{o,d}^- + v_{o,d}^+v_{o,q}^- \\ v_{o,q}^+v_{o,d}^- + v_{o,d}^+v_{o,q}^- & v_{o,q}^+v_{o,q}^- - v_{o,d}^+v_{o,d}^-\end{bmatrix}\begin{bmatrix} i_{v,d}^+ \\ i_{v,q}^+\end{bmatrix} \tag{5}$$

where k^- is used to select the desired power flow characteristics. Thus, a value of k^-=0 corresponds to BPSC, k^-=−1 corresponds to CAP, and k^-=1 results in CRP. The voltage components in the equation are transformed to the positive or negative sequence reference frames by using the VSM phase angle.

The other two strategies for negative sequence current control in [19], [20] were based on a virtual impedance (VI), equivalent to (4). Thus, for these cases, the negative sequence current reference is calculated as:

$$\mathbf{i}_{v,NSVI}^{-,*}=\frac{\mathbf{v}_e^{-*}-\mathbf{v}_o^{-}}{r_{VI}^{-}-j\omega_{VSM}l_{VI}^{-}}, \tag{6}$$

where $\boldsymbol{v}_e^{-*}$ is the negative sequence voltage reference. If $\boldsymbol{v}_e^{-*}$ is set to zero, this results in a pure Negative Sequence Virtual Impedance (NSVI) control. However, the *d*- and *q*-axis components of $\boldsymbol{v}_e^{-*}$ can also be defined by a closed loop control of the negative sequence voltage. In this case, Negative Sequence Voltage Control (NSVC) is obtained by applying PI-controllers to provide the *d*- and *q*-axis components of $\boldsymbol{v}_e^{-*}$ that will force the amplitude of $\mathbf{v}_o^-$ to zero.

D. Circulating current and energy control loops

The applied strategy for MMC energy control was first proposed in [18], and was applied without further analysis in [20]. An overview of the individual control loops for energy balancing and the cascaded inner loop circulating current control, expanded from Fig. 1, is shown in Fig. 3. The basic principles for modelling the internal MMC dynamics according to [25] are utilized for the design of the control structure. Thus, the average energy sum of each phase is controlled by utilizing the dc-component of the circulating current while the average energy difference between the upper and lower arms is controlled by the fundamental frequency component of the circulating current. This can also be understood from the equivalent dynamics of the energy sum and energy difference in each phase *k*, which is given as [18], [26]:

$$\frac{dW_{C,k}^{\Sigma}}{dt}=\frac{dW_{C,u,k}}{dt}+\frac{dW_{C,l,k}}{dt}=I_{cir,k}\left(V_{dc}-2V_{cir,k}\right)-I_{v,k}V_{v,k}, \tag{7}$$

$$\frac{dW_{C,k}^{\Delta}}{dt}=\frac{dW_{C,u,k}}{dt}-\frac{dW_{C,l,k}}{dt}=I_{v,k}\left(\frac{V_{dc}}{2}-V_{cir,k}\right)-2I_{cir,k}V_{v,k}. \tag{8}$$

Here, W refers to the energy stored in the equivalent capacitance, while Σ and Δ refer to the sum and difference of quantities related to the upper (u) and lower (l) arms, respectively. Furthermore, I_{circ} is the circulating current, while V_{circ} is the voltage driving the circulating current [18].

It should be noted that a Proportional-Integral-Resonant (PIR) controller with two resonant terms, i.e., at the fundamental frequency and at the second harmonic frequency, is adopted for circulating current control according to [26]. The resonant terms of the PIR controllers are implemented according to [21], and are kept frequency-adaptive by the VSM speed.

1) Energy sum control

The energy sum is regulated by a PI-controller operating on the average value of the squared capacitor voltage of each phase leg [18], [25]. The resulting control loop for each phase is shown in Fig. 4, illustrating how the reference value $\bar{v}_C^*$ for the average arm capacitor voltage is squared and multiplied by 2 to give a reference signal that is proportional to the desired

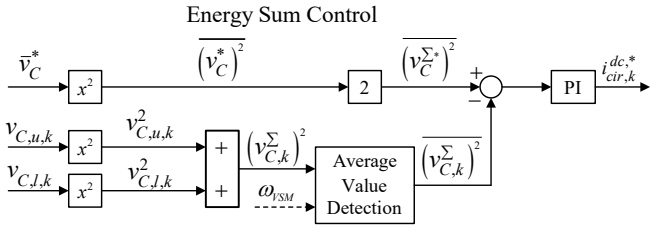

Fig. 4 Implementation of energy sum control for the MMC [18]

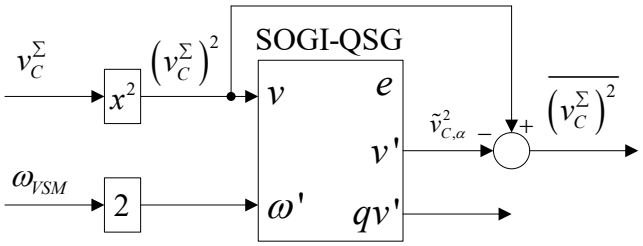

Fig. 5 SOGI-QSG-based notch filter for average value detection of sum energy

energy sum per leg. Similarly, the measured arm capacitor voltages v_C are squared before calculating the sum of the upper and lower arms, $(v^{\Sigma}_C)^2$. The resulting signal is then proportional to the instantaneous energy sum in each leg and will contain a dc component as well as a dominant second harmonic oscillation [25]. Since only the dc-component of this signal should be used as a feedback signal for controlling the average energy sum, a filtering technique for average value detection is required. Thus, the dc component of the energy signal, i.e. $(\bar{v}^{\Sigma}_C)^2$, is obtained and used for comparison with the reference signal $(\bar{v}^{\Sigma *}_C)^2$. Finally, the PI controller generates the dc-component of the circulating current reference $i_{cir}^{dc,*}$.

2) Energy difference control

The energy difference control requires some additional considerations compared to the energy sum control, to ensure that power oscillations are not allowed to propagate into the dc-bus under unbalanced conditions. However, the starting point is the difference between the square of the upper and lower equivalent arm capacitor voltages of each phase, i.e. $(v^{\Delta}_C)^2$. This signal contains a significant fundamental frequency ripple which must be filtered out to detect its average value $(\bar{v}^{\Delta}_C)^2$. The average of the energy difference in each phase is then regulated to the reference value of zero by using a PI controller, in the same way as for the energy sum control. However, the outputs from the PI controllers are dc signals, while a fundamental frequency circulating current is needed for regulating the energy difference within the MMC legs [25].

As further explained in [18], on the basis of [27], [28], the average value (i.e. the zero sequence) of the energy difference for the three phases can be controlled by using the positive sequence *d*-axis circulating current. Furthermore, the *d*- an *q*-axis negative sequence circulating currents can be used to compensate for deviations in the energy difference between the three phases. Thus, the reference signals for the positive and negative sequence fundamental frequency circulating current components can be calculated from the output of the three PI-controllers as given by (9) and (10).

$$i_{cir,d}^{+\omega,*} = -\underbrace{\frac{i_a^{PI_\Delta} + i_b^{PI_\Delta} + i_c^{PI_\Delta}}{3}}_{i_z^{PI_\Delta}}, \tag{9}$$

$$i_{cir}^{-\omega,*} = \underbrace{\frac{2i_a^{PI_\Delta} - \left(i_b^{PI_\Delta} + i_c^{PI_\Delta}\right)}{3}}_{i_\alpha^{PI_\Delta} = i_{cir,d}^{-\omega,*}} + j \cdot \underbrace{\left(\frac{1}{\sqrt{3}} \cdot \left(i_c^{PI_\Delta} - i_b^{PI_\Delta}\right)\right)}_{i_\beta^{PI_\Delta} = i_{cir,q}^{-\omega,*}}. \tag{10}$$

In these equations, the superscripts PI_Δ refers to the output of the PI-controllers, while the superscripts $+\omega$ and $-\omega$ refers to the positive and negative sequence reference frames defined by the VSM phase angle θ_{VSM}. These reference signals are transformed to the *abc* frame and added together to provide the fundamental frequency circulating current references for each phase that are used as an input to the PIR-controllers in Fig. 3.

III. FILTERING STRATEGIES FOR AVERAGE VALUE DETECTION IN THE ENERGY CONTROL LOOPS

As seen from Fig. 3 and Fig. 4, the control of the energy sum and energy difference depends on the average value detection of the feedback signals. This average value detection influences the dynamic performance and bandwidth of the energy control loops. In previous literature, the average value detection is usually based on fixed frequency notch filters (FF-NF), as applied in [7], [15]-[17], [29], or a MAF with fixed filter window width as applied in [27], [30], [31].

The notch-filtering approach can only be applied for the energy sum and energy difference, where single frequency sinusoidal oscillations occur. Instead, MAFs can also be applied directly in the equivalent arm capacitor voltages, or in their squared values, which contain multiple harmonic components. Since fundamental frequency oscillations appear in the arm voltages, a window width of one fundamental frequency period will then always be needed. However, if MAF filtering is applied in the sum and difference of the arm capacitor energies, the window width can be selected according to the single dominant frequencies to be filtered out. In any case, the use of MAFs for the average value detection introduces an equivalent delay in the range of half the window width of the filter [32].

As first proposed in [18], inspired by [33], a frequency-adaptive notch filter based on SOGI-QSGs can be used for the average value detection in the energy control. As demonstrated by simulations in [18], the frequency-adaptivity will be important for VSM-based control in islanded operation or in weak grids where normal operation during frequency deviations up to 2-3 Hz might be required [34]. Furthermore, the SOGI-QSG-based implementation can reduce the equivalent delay in the feedback signals of the energy controllers compared to MAF-based implementations.

In order to remove the second-order harmonic in the feedback signal for the sum energy control, a SOGI-based adaptive notch filter is used as shown in Fig. 5. The figure shows how the square of the voltage sum and a frequency given by twice the VSM angular frequency are used as inputs for a SOGI-QSG. Then, the in-phase output signal from the SOGI-QSG is the second harmonic component of a signal

proportional to the energy sum. Subtracting the isolated second harmonic oscillating component from the input signal to the SOGI-QSG results in a notch filter effect that eliminates the second harmonic component from the feedback signal used for the sum energy control. Considering the transfer function for the in-phase (or α-axis) path of a SOGI-QSG according to [23], the expression for the notch filtered output signal is given by:

$$\overline{\left(v_C^{\Sigma}\right)^2} = \underbrace{\frac{s^2+\left(2\Omega_b\omega_{VSM}\right)^2}{s^2+k\cdot 2\Omega_b\omega_{VSM}+\left(2\Omega_b\omega_{VSM}\right)^2}}_{h_{SOGI}^{notch}(s)}\left(v_C^{\Sigma}\right)^2, \tag{11}$$

where Ω_b is the base value for the angular frequency (i.e. $2\pi F_b$ with base frequency F_b of 50 Hz), and k is the internal gain of the SOGI-QSG. The value of k is set to $\sqrt{2}$, as an optimal trade-off between transient response and filtering capability [35].

For analysing the impact of the required filtering in the feedback signals, the closed loop circulating current control can be assumed to have much higher bandwidth than the outer loop energy controllers. Thus, the dc-component of the circulating current is assumed to be equal to the current reference output of the PI controller in Fig. 4. Furthermore, the sum capacitor energy is the integral of the power transferred by the circulating current, given by $v_{dc}\cdot i_{cir}^{dc,*}$. However, the feedback signal is the squared voltage, which is related to the energy by ½ $C\cdot V^2$. Considering per-unit representation of the signals, the time constant T_C of the energy integral in the control loop can then be expressed from the equivalent arm capacitance C and the base value for voltage and current as:

$$T_C = \frac{1}{2v_{dc}}\frac{V_b C}{I_b} = \frac{1}{2v_{dc}}\frac{V_b C_{SM}}{I_b N}. \tag{12}$$

Thus, the open loop transfer function from the reference signal $(\bar{v}^{\Sigma *}_C)^2$ to the measured average value of the squared sum capacitor voltage, $\overline{\left(v_C^{\Sigma}\right)^2}$ can be approximated as:

$$h_{OL,SOGI}^{\Sigma}(s) \approx \underbrace{K_p\frac{1+T_i\cdot s}{T_i\cdot s}}_{\text{PI-controller}}\cdot\underbrace{\frac{1}{T_C\cdot s}}_{\substack{\text{Equivalent}\\ \text{capacitance}}}\cdot h_{SOGI}^{notch}(s). \tag{13}$$

Similarly, the open loop transfer function when the average value detection is based on a MAF, can be expressed as:

$$h_{OL,MAF}^{\Sigma}(s) \approx \underbrace{K_p\frac{1+T_i\cdot s}{T_i\cdot s}}_{\text{PI controller}}\cdot\underbrace{\frac{1}{T_C\cdot s}}_{\substack{\text{Equivalent}\\ \text{capacitance}}}\cdot\underbrace{\frac{1-e^{-T_w\cdot s}}{T_w\cdot s}}_{\text{MAF}}. \tag{14}$$

A comparison of the Bode diagrams for the two open loop transfer functions given by (13) and (14) is shown in Fig. 6. The plots are based on the parameters given in Table I, and clearly show how the case with the SOGI-based notch filter has a higher phase margin than the case with the MAF. Indeed, for the specific controller parameters, the phase margin with the SOGI-based notch filter is 66.2° while it is about 44.6° with the MAF. It should be noted that this difference is mainly caused by the characteristics and tuning of the SOGI-QSG. However, filtering with a single notch frequency is only applicable to the energy sum and difference

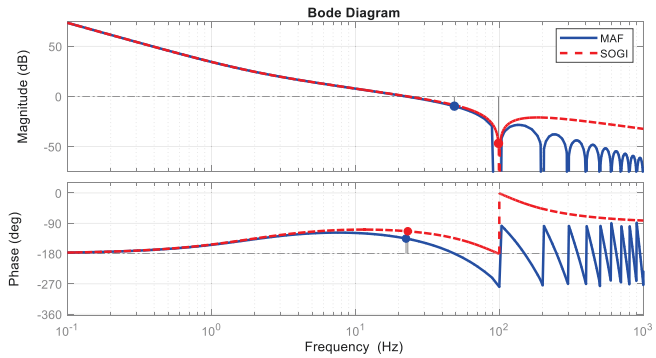

Fig. 6. Bode diagram of open loop transfer function for sum energy control with MAF of SOGI-based notch-filter in the feedback

signals where the oscillations are separated into individual sinusoidal components. Thus, if the feedback signals are based on the squared arm capacitor voltages, two notch filters at 50 Hz and 100 Hz, or a MAF with a fundamental frequency window of 20 ms, will be required. This will further reduce the bandwidth or phase margin of the energy control. In this specific case, the phase margin would be reduced to 15.6 ° if a MAF with 20 ms window was used with the same controller parameters. It should also be noted that the use of a MAF would be necessary if the equivalent arm capacitor voltages, or the sum and difference of the arm capacitor voltages, would be used as feedback signals, since the nonlinearity between power flow and capacitor voltage implies that the individual frequency components will not be purely sinusoidal signals.

The implementation and analysis will be similar for the energy difference controller, with the main difference that a fundamental frequency component must be filtered out. Thus, the SOGI-QSGs will be tuned for the frequency of ω_{VSM} instead of the second harmonic frequency and the equivalent MAF will have a window of 20 ms.

IV. CONFIGURATIONS FOR SIMULATIONS AND EXPERIMENTAL VERIFICATION

The performance of the presented energy control strategy, including the impact from the different options for feedback signal filtering has been assessed by numerical simulations and by experimental tests on a laboratory scale prototype.

A. Simulated HVDC-scale configuration

An MMC operated as a power-controlled terminal of an HVDC transmission system has been modelled and simulated numerically in the Matlab/Simulink environment. For simplicity, the ac-side of the MMC is connected to an equivalent grid model that includes a local load and an ideal voltage source behind a series impedance, as indicated in Fig. 1. The MMC is represented with an average model that captures the aggregated dynamics at the arm level by assuming ideal balancing between the cells. The parameters used for the simulations are presented in Table I, where the circuit parameters are adapted from [36]. The numerical simulation of the electrical circuit is conducted with a time step of 5 µs while the control system is simulated with a time step of 70 µs.

TABLE I – PARAMETERS FOR ANALYSIS AND SIMULATION

MMC data	
Nominal power , P_{nom}	1000 MW
Nominal line-to-line grid voltage, $V_{g,nom}$	333 kV
Nominal dc side voltage, V_{dc}	640 kV
Number of modules per arm, N	400
Arm inductor, l_f	50 mH
Submodule capacitance, C_{SM}	10 mF
Transformer inductance L_T	28.2 mH
Transformer resistance R_T	0.9 Ω
Control parameters	
Frequency droop coefficient, k_w	20 pu
Frequency damping factor, k_d	200 pu
Virtual inertia, T_a *(2H)*	10 s
Reactive power droop coefficient, k_q	0 pu
Voltage limiting factor, $k_{v,\text{lim}}$	1.05
Positive Sequence Virtual Impedance, l_{VI}^+, r_{VI}^+	0.2 pu, 0.01 pu
Negative Sequence Virtual Impedance, l_{VI}^-, r_{VI}^-	0.4 pu, 0.02 pu
AC-side PR Current Controller $k_{c,P}$, $k_{c,R}$	0.8 pu, 0.3 pu
Negative Sequence Voltage Control, $k_{P,NS}$, $k_{i,NS}$	0.3 pu, 5 pu
Circulating Current Controller, $k_{cc,P}$, $k_{cc,i}$, $k_{cc,R(w)}$, $k_{cc,R(2w)}$	0.9 pu, 630 pu 0.06 pu, 0.08 pu
Sum Energy Control, $k_{P,\Sigma}$, $k_{i,\Sigma}$	0.5 pu, 6 pu
Energy Difference Control, $k_{P,\Delta}$, $k_{i,\Delta}$	0.6 pu, 6 pu

TABLE II – PARAMETERS OF EXPERIMENTAL SETUP

Rated power	50 kVA
Rated line-to-line grid voltage	400 V
Rated dc voltage	700 V
Number of modules per arm	12
Module capacitance	15 mF
Arm inductance	1.4 mH
Control time-step	80 us

B. *Experimental setup*

Experimental results are obtained from an MMC prototype with parameters as listed in Table II. The prototype is designed for power levels up to 50 kVA at 400 V line-to-line rms voltage, but, for convenience, the experiments are conducted at reduced voltage, as shown for each individual test. The laboratory setup was configured according to Fig. 7, which presents a schematic overview of the ac- and dc-side interfaces of the converter under test, as well as an overview of the control system implementation. A COMPISO switch-mode amplifier from EGSTON Power is used as a grid emulator to impose the ac-side voltages for the MMC, including the unbalanced conditions, when operated in grid connected mode. Two separate terminals from the same amplifier is also providing the dc voltage for the converter. The configuration also includes a transformer for galvanic separation, circuit breakers and a resistive load for testing in islanded operation. An OPAL-RT real-time simulation platform is utilized for implementing the control system and is sending arm voltage references to the local distributed arm-level control of the MMC prototype via fiber-optic links. The internal balancing control of each arm is implemented in a dedicated control board integrated into the converter hardware. It should be noted that the insertion indices for each arm are calculated from the voltage references V_v^* and V_{cir}^* by using the actual arm voltages, according to [25].

Further details about the MMC prototype and the control hardware of the experimental setup are available in [20], while the details on the modulation and distributed control of the individual modules in each arm are described in [12]. A photo of the experimental setup, with indications of the main elements, is shown in Fig. 8.

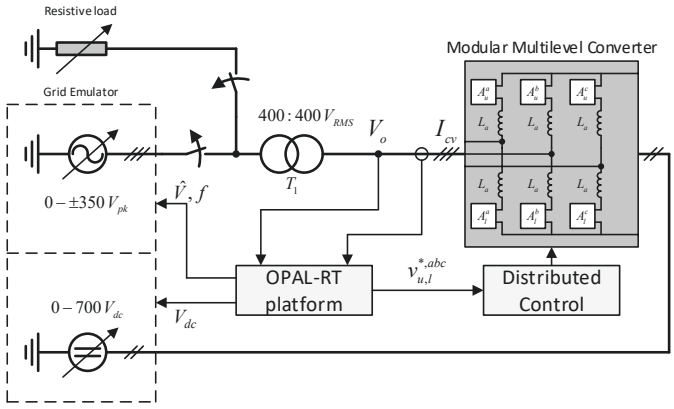

Fig. 7. Schematic overview of experimental setup

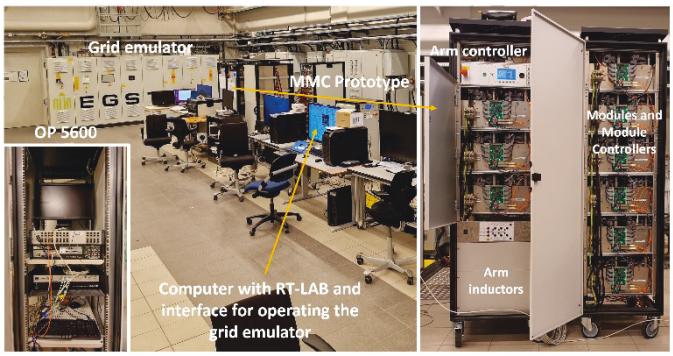

Fig. 8. Photo of laboratory facility with the experimental setup

The experiments are conducted in a rather flexible laboratory environment with multiple busbars and breakers that allow for reconfigurable connections, and the grid emulator allows for easily imposing unbalances in the ac voltages and/or variations in the grid frequency. The converter prototype is designed to be representative of the main features of an MMC, and the main parameters are scaled from [36], as described in [37]. However, due to practical constraints, the characteristics differ from a full-scale converter in a few aspects. For instance, the number of modules per arm is limited to 18 while a converter for HVDC applications generally presents a higher number. Furthermore, the switching devices have been intentionally oversized in the design phase to reduce the equivalent resistances. However, the conduction losses in the switches and losses in the capacitors are still rather large in per unit compared to a full-scale converter. Thus, the prototype can generally be expected to have a slightly more damped behavior than what could appear in an industrial MMC HVDC terminal.

V. IMPACT OF FILTER CHARACTERISTICS AND FREQUENCY ADAPTIVITY IN THE ENERGY CONTROL LOOPS

This section focuses on the transient response to grid frequency variations and on the steady-state performance during operation with large deviations from the nominal frequency. All following cases are obtained with ac-side

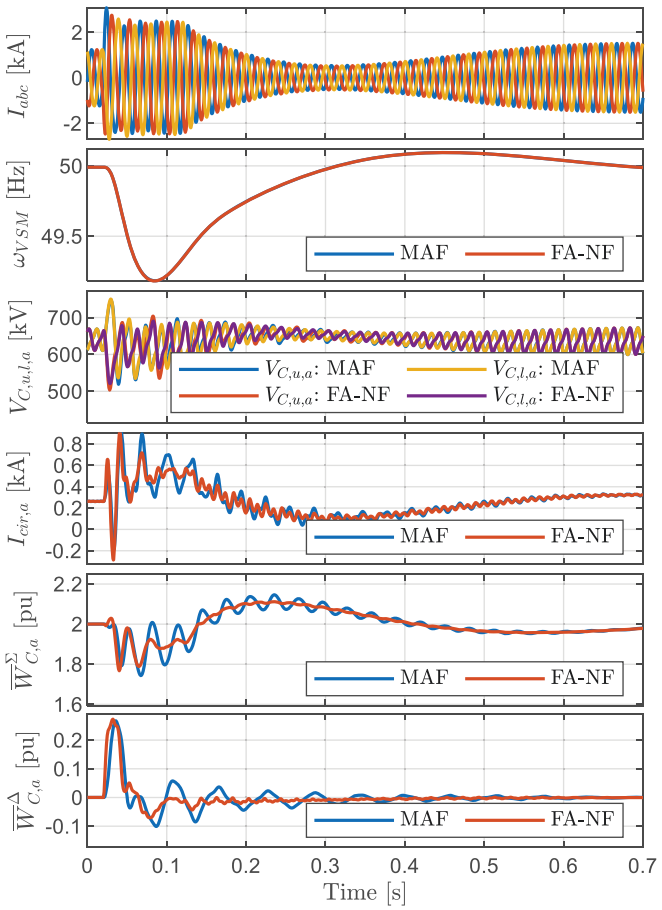

Fig. 9. Simulation results showing the response to a −30° phase shift in the grid voltage while operating at a grid frequency of 49.9 Hz (0.998 pu) with MAF-based and SOGI-QSG-based FA-NF in the energy control

control for obtaining Balanced Positive Sequence Currents, while operation with different negative sequence current control strategies is assessed in section VI.

A. *Simulation results with HVDC scale parameters*

Firstly, the performance of the proposed MMC energy control strategy with SOGI-based frequency-adaptive feedback filtering is assessed in comparison to MAF-based filtering. Furthermore, the impact of the frequency adaptivity in the notch filtering, and in the circulating current control, on the steady-state operation, is also evaluated.

1) Response to changes in grid voltage phase and influence of feedback signal filtering for the energy control

A set of simulations results presented in Fig. 9 illustrate the impact of the filtering methods in the energy control loops on the dynamic response of the internal MMC variables during grid-connected operation. The system is assumed to operate with a frequency of 49.9 Hz (0.998 pu) and a power reference of 0.4 pu (400 MW) when a step in the grid voltage phase angle of −30° is introduced at time t=0.02 s. During the initial transient after the perturbation, the limit for the positive sequence currents is reached, as seen in the first plots of Fig. 9. As soon as the current references fall below the limitation, the regular inertial response of the swing equation can be clearly seen in the results. Although the currents are only shown as obtained with the SOGI-QSG-based FA-NF, the ac-side response with MAF-based energy control is almost identical. Indeed, the VSM-based control of the ac-side is not significantly influenced by the MMC energy control as long as it is stable, and the capacitor voltages are maintained with the regular operating range.

The results in Fig. 9 clearly illustrate how the settling time and damping of the average sum energy and energy difference are improved in the case of the FA-NF compared to the MAF. For the simulated conditions, using the same controller gains for both cases, the settling time of the dominant oscillation in the average energy components is reduced from around 0.5 s with the MAF to less than 0.2 s with the FA-NF. This improvement is mainly associated with the increased phase margin identified in Fig. 6. Although these results are obtained with the same controller parameters applied to two systems with different frequency characteristics, they imply that a re-tuning of the energy control to achieve a more damped response with the MAF will result in a longer settling time and potentially in higher overshoot in response to perturbations. It can also be noted that a FF-NF, as used in [7], [17], [29], could provide the same phase margin and the same transient response as the FA-NF when operated at nominal frequency. However, the filtering performance will be degraded during frequency variations, as demonstrated in the following.

2) Impact of frequency adaptivity

Fig. 10 and Fig. 11 compare the steady state response of the currents, voltages, and average energy components when different degrees of frequency adaptivity are applied in the energy control and in the circulating current control. The simulations are obtained with a frequency deviation of −1 Hz (i.e., operation at 49 Hz) and an active power reference of 0.5 pu, resulting in 0.7 pu of active power flow due to the VSM frequency droop. The compared cases include the use of a MAF, FA-NF and FF-NF in the feedback signals of the energy controllers, as well as a case where a FF-NF is used in combination with fixed-frequency resonant terms in the circulating current controller (i.e., FF-CCC). From the results in Fig. 10, it can be noticed that the ac-side currents and voltages are not significantly affected by the changes in the frequency adaptivity of the internal control. This is largely due to the compensated modulation strategy according to [25], [38], which is applied in the control system to decouple the arm output voltages from the arm capacitor voltage oscillations.

The time-domain plots in Fig. 10 and the corresponding harmonic analysis in Fig. 11 confirm how the FA-NF is clearly the most effective strategy for eliminating the dominant oscillation frequency from the average sum energy and energy difference signals. The results show how the MAF is effectively removing noise but retains a noticeable fundamental frequency oscillation when the window width does not coincide with the actual frequency component to be filtered out. The figures also demonstrate the importance of VSM-based frequency-adaptivity in the circulating current controllers, as the case of FF-NF with FF-CCC shows a significant increase in the 2nd harmonic component of the

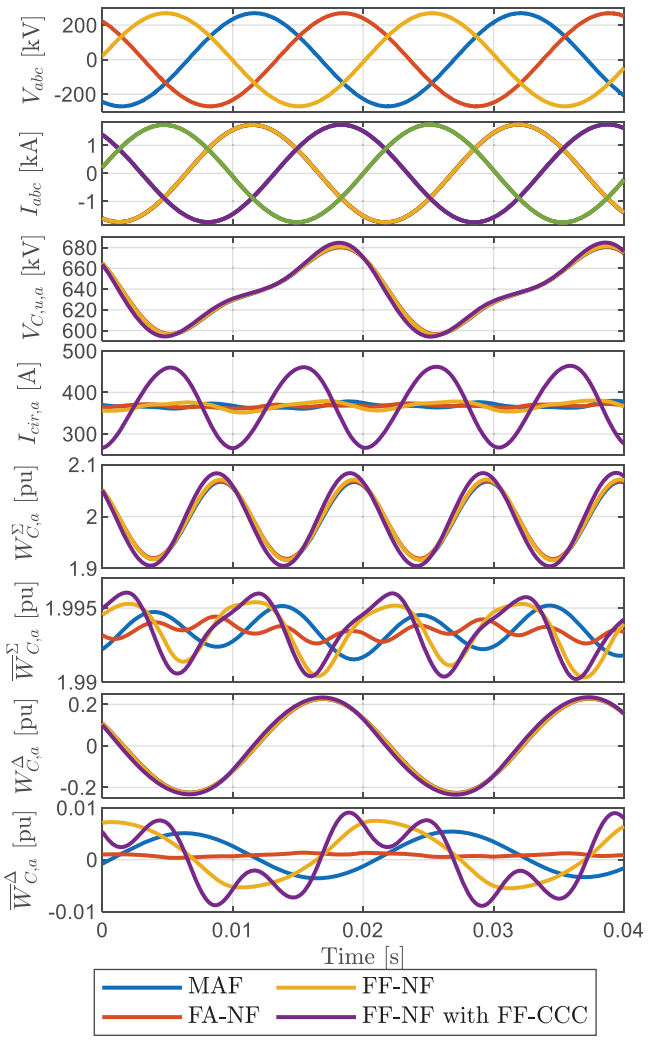

Fig. 10. Simulation results demonstrating the difference in steady-state performance with different energy filtering strategies and the impact of frequency adaptivity in the control when operating at 49 Hz

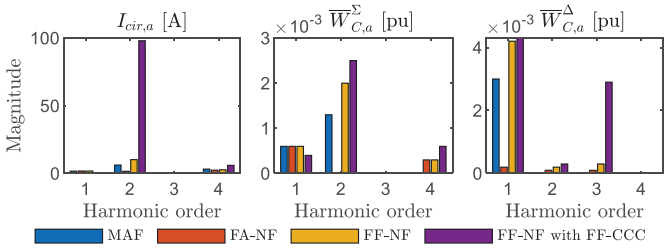

Fig. 11 Harmonic analysis of the circulating current and the detected average energy signals from the simulation results shown in Fig. 10

circulating currents, which results in a 3rd harmonic component in the energy sum.

B. Experimental results

The observations from the simulation results regarding the impact from the filtering strategy on the transient response and the steady-state performance during frequency deviations are also verified by corresponding experiments.

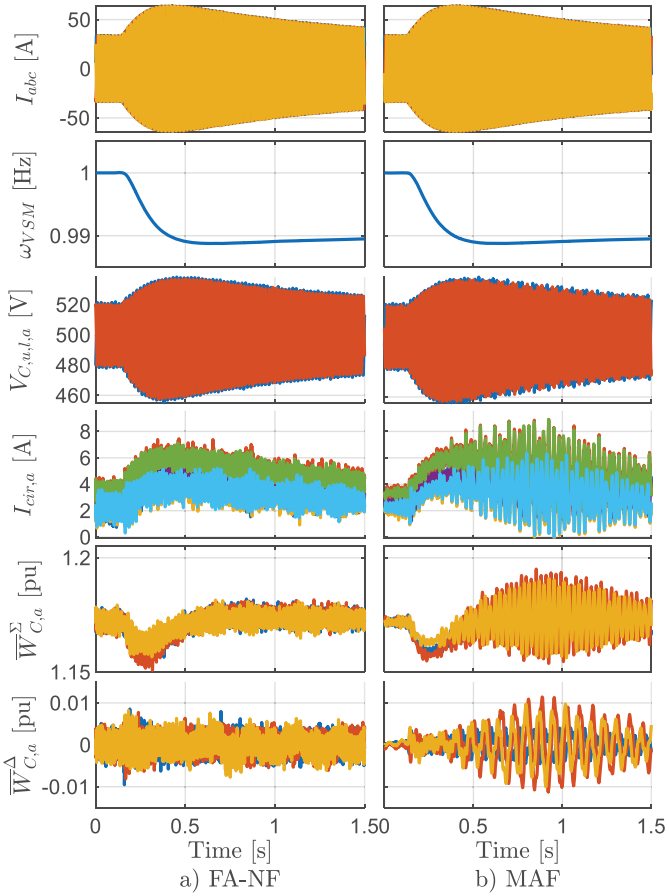

Fig. 12. Experimental results for comparison of response to a grid frequency step of −0.01 pu (0.5 Hz) with different filtering strategies in the feedback signals for the energy control loops; (a) SOGI-based FA-NF, and (b) Moving Average Filter (MAF).

1) Impact of filtering strategy in the energy control loops on the internal dynamics of the MMC

Results from experimental comparison of the transient response with the SOGI-QSG-based FA-NF and the MAF-based average value detection are presented in Fig. 12 The test is conducted with the grid emulator imposing a 25% voltage unbalance at reduced voltage. A step in the grid frequency from 1 pu to 0.99 pu is imposed at time t = 0.15 s. The results show how the ac currents are well balanced in both cases. However, when using the same controller parameters, the circulating currents, the energy sum and the energy difference signals appear smoother and significantly more damped with the SOGI-QSG-based FA-NF than with the MAF. This confirms how the reduced equivalent delay resulting from the SOGI-QSG-based filtering can improve the dynamic response of the control loops. Further optimization of the tuning with the different filtering methods is beyond the scope of this paper.

2) Impact of frequency-adaptivity on steady-state operation

To further verify the impact of the frequency-adaptivity in the energy filtering on the operation during frequency deviations, a test is conducted for steady-state operation at 47.5 Hz (0.95 pu). This condition corresponds to the lower

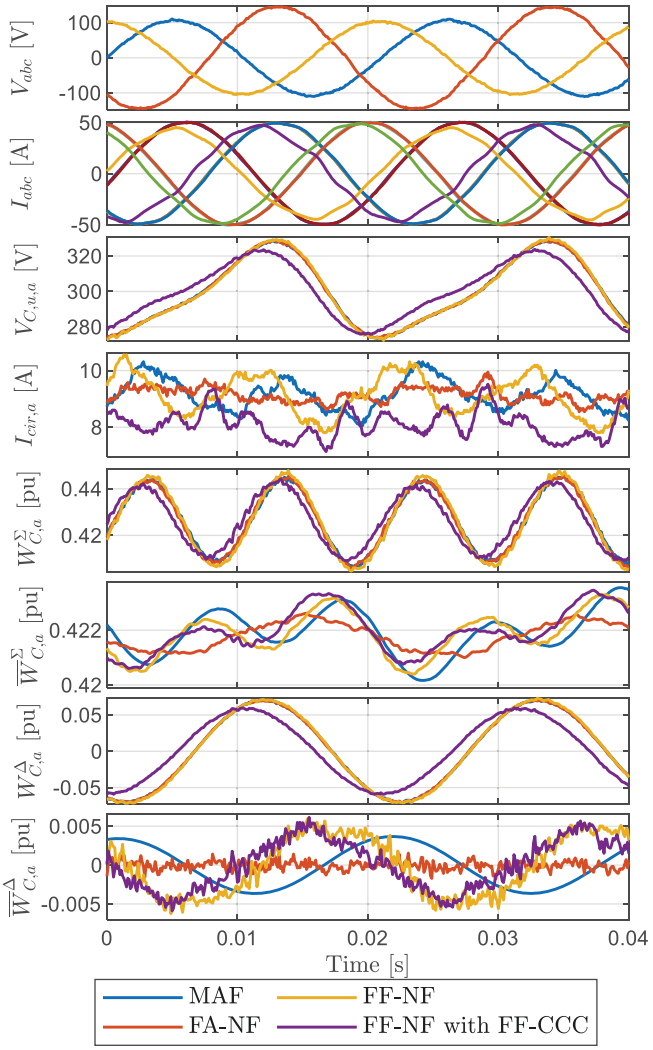

Fig. 13. Experimental results showing the difference in steady-state performance with different energy filtering strategies and the impact of frequency adaptivity in the control when operating at 47.5 Hz

frequency limit where continuous operation is required in several isolated power systems [34]. The time-domain signals obtained for the same cases as evaluated by simulation are presented in Fig. 13. The results are in line with the general observations from the simulations, although the higher order harmonics in the average energy signals are less dominant in the experimental case where the frequency adaptivity is disabled in both the energy control feedback signals and in the circulating current controllers. However, the results verify how only the FA-NF can effectively eliminate the fundamental frequency components of the energy difference. From the Fourier analysis presented in Fig. 14, it is also clear that the FA-NF is effectively filtering out the second harmonic component in the average energy sum, while a significant second harmonic component is remaining for all the other strategies. Although the amplitudes of these signals are small for the presented testing conditions, they could have a more significant impact for testing at higher power levels and in MMCs with lower capacitance values.

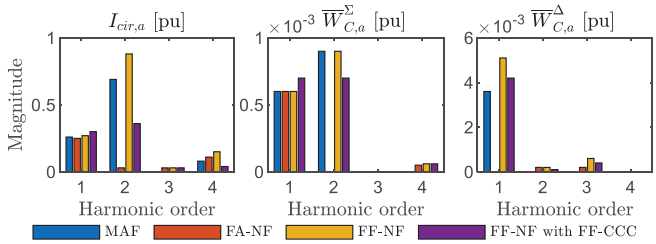

Fig. 14 Harmonic analysis of the circulating current and the detected average energy signals from the experimental results shown in Fig. 13

VI. VERIFICATION OF ENERGY CONTROL PERFORMANCE WITH DIFFERENT AC-SIDE CONTROL STRATEGIES

While all results in section V. were obtained with BPSC control on the ac-side, the studied energy control strategy with SOGI-based FA-NFs is designed to be applicable independently of the strategy for controlling negative sequence currents under unbalanced conditions. This is verified by the following simulations and experiments.

A. Simulation of islanding event

To verify the performance of the MMC during both grid connected and islanded operation, the transient of an islanding event under unbalanced conditions is simulated. Unbalanced islanded conditions are created by a balanced delta-connected load with impedances Z_L (10 pu and cos ϕ=0.99) and an additional load between phase *a* and *b* with an impedance of 0.5 Z_L. Before the islanding, the PCC is initially connected to an ideal voltage source supplying all the unbalanced currents, which is then disconnected at t = 0.03 s. Fig. 15 shows the voltages and currents as well as the active and reactive power flow, the equivalent capacitor voltages of phase *a* and the circulating currents for the five negative sequence control strategies analyzed in [20].

Detailed discussion of the VSM performance under the same conditions are presented in [20], highlighting how the BPSC, CAP and CRP strategies are not suitable for islanded operation. However, the capacitor voltages plotted in Fig. 15 confirm that the energy control loops work as intended in all cases by regulating the arm energies to their reference values independently of the voltage unbalance and the strategy for controlling the negative sequence currents. Furthermore, the circulating currents settle to dc-components in steady state and illustrate how much power is transferred in each phase. For instance, it is clearly seen how the CAP strategy provides the same circulating current dc component, implying the same active power flow, in all the three phases. Furthermore, the circulating current (and the active power transfer) is higher for the cases of Negative Sequence Virtual Impedance (NSVI) and Negative Sequence Voltage Control (NSVC) compared to the other three control strategies. This is a result of these two strategies reducing or eliminating the voltage unbalances and supplying the full load in all the phases. The figure also shows that the settling time of the transients in the arm voltages and the circulating currents are consistent and almost independent from the applied strategy for ac-side control.

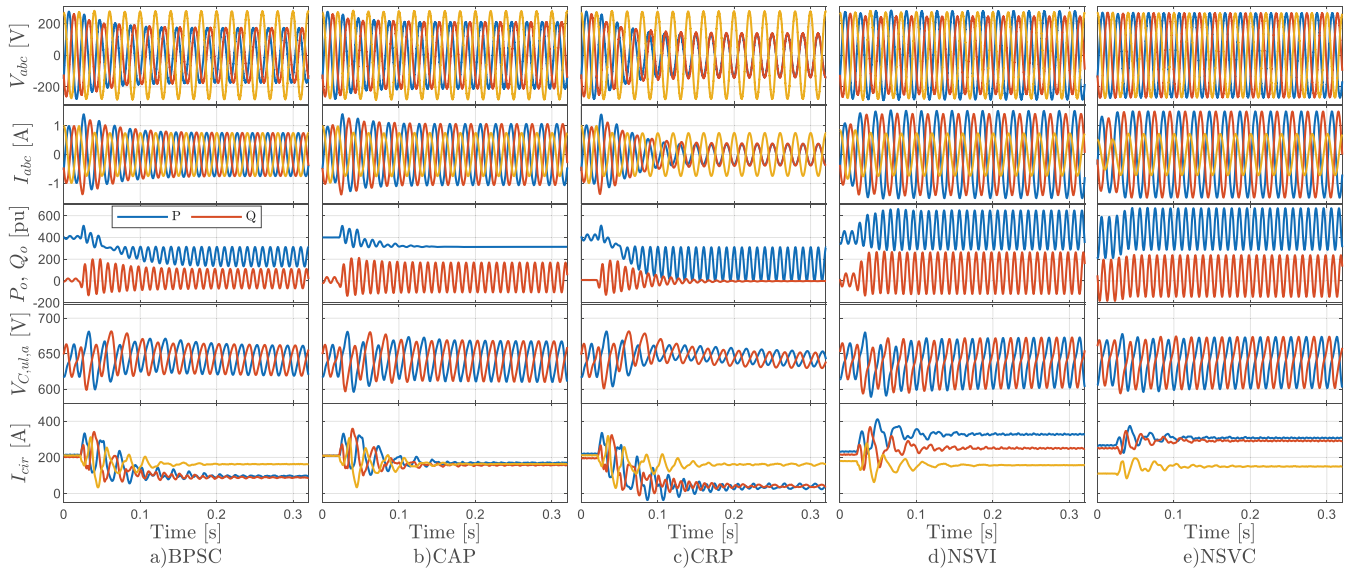

Fig. 15. Simulation results demonstrating the response to islanding under unbalance grid with different strategies for ac-side negative sequence current control, a) Balanced Positive Sequence Currents (BPSC), b) Constant Active Power (CAP), c) Constant Reactive Power (CRP), d) Negative Sequence Virtual Impedance (NSVI), e) Negative Sequence Voltage Control (NSVC)

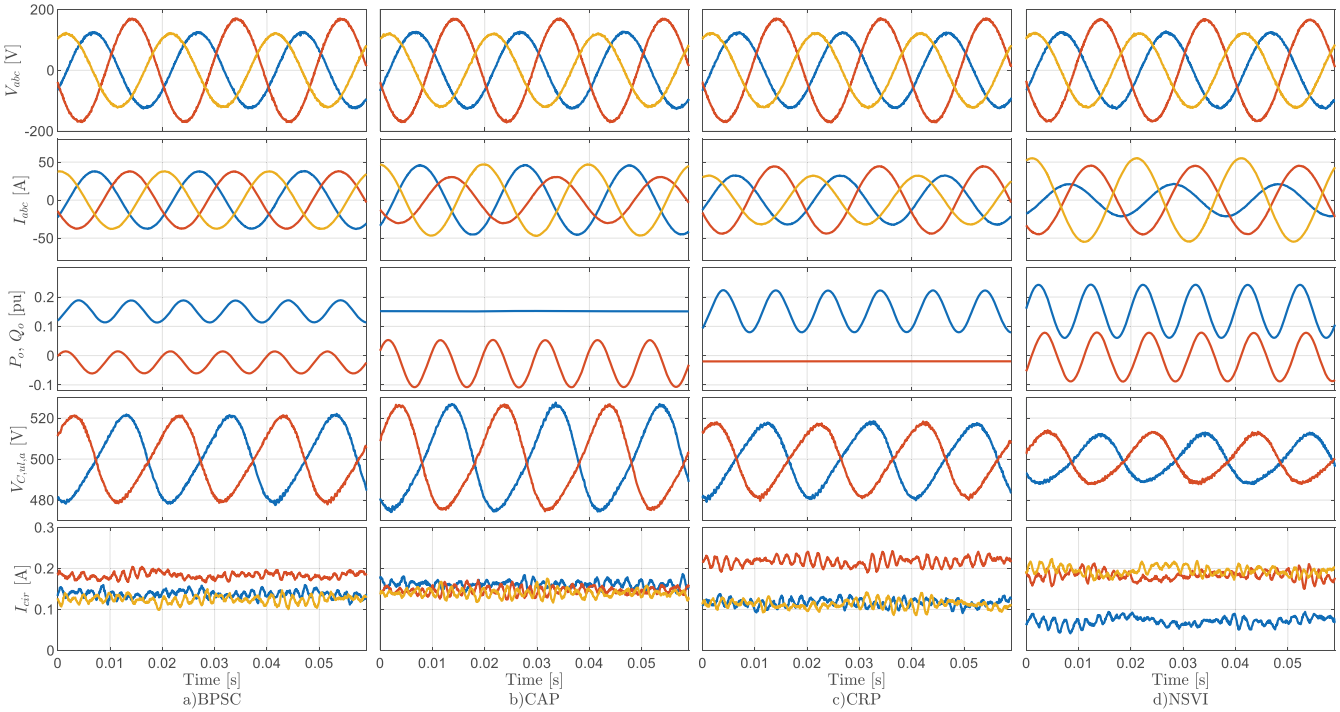

Fig. 16. Experimental results with different strategies for negative sequence current control under unbalanced conditions, a) Balanced Positive Sequence Currents (BPSC), b) Constant Active Power (CAP), c) Constant Reactive Power (CRP), d) Negative Sequence Virtual Impedance (NSVI), e) Negative Sequence Voltage Control (NSVC)

B. Experimental results

Experimental results at steady state conditions with four different strategies for controlling the negative sequence currents (i.e. BPSC, CAP, CRP, NSVI) are shown in Fig. 16. The tests are performed with a 25% voltage unbalance imposed by the grid emulator. The NSVC is not tested, as it is not applicable in strong grid conditions.

The results in Fig. 16 clearly demonstrate that the control objectives are fulfilled, and that the converter operates as expected in steady state. Indeed, the arm capacitor voltages are controlled to their reference values independently from the voltage unbalances and the control of the ac-side currents.

While the results in Fig. 16 demonstrate the expected steady-state operation, a set of results showing the response to a transient event during grid connected operation is shown in Fig. 17. The transient is the same step of −0.01 pu (0.5 Hz) in

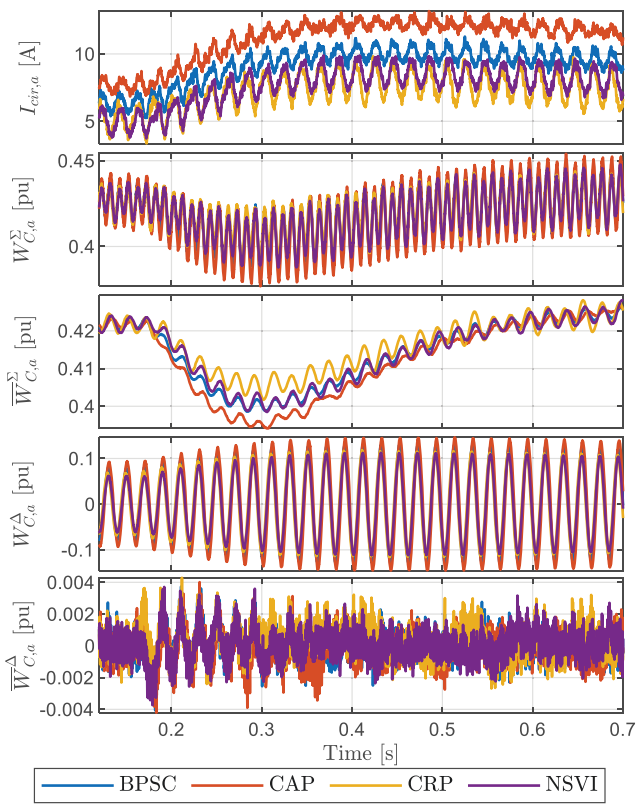

Fig. 17 Experimental verification of transient response in the circulating current and energy signals to a grid frequency step of −0.01 pu (0.5 Hz) with different AC-side control strategies under unbalance grid connected operation (curves are shown only for phase a)

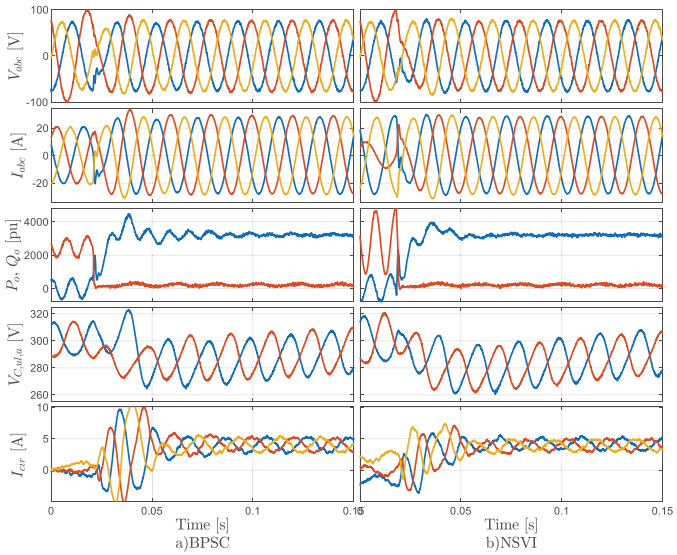

Fig. 18 Experimental results showing the response to a sudden islanding event when the VSM is operated under unbalanced conditions with ac-side control for a) Balanced Positive Sequence Currents (BPSC), or b) Negative Sequence Virtual Impedance (NSVI)

the frequency of the grid emulator as applied in Fig. 12. The figure shows that the perturbation of the energy control in phase *a* is slightly different among the 4 applicable strategies for negative sequence current control. This is mainly because the power flow in each of the phases depends on the ac-side control strategy. However, the figure also shows that the settling time of the transient is consistent and independent from the strategy for negative sequence current control.

Finally, the islanding operation of the VSM-controlled MMC is also tested for operation with BPSC and NSVI. Due to practical constraints, only experiments with a balanced load are conducted. Furthermore, the operation with CAP or CRP is not tested since these strategies are not practically relevant for islanded operation, while the case of NSVC is not tested because it is inapplicable for strong grid operation before the islanding event. The results from the two conducted tests are shown in Fig. 18 and demonstrate how the energy control strategy is operated as intended and brings the MMC arm voltages and circulating currents into the new operating condition with a similar transient as in grid connected operation. Thus, the results experimentally confirm how the presented control strategy maintains the intended performance in the full range of expected operating conditions.

VII. CONCLUSIONS

This paper presents a frequency adaptive energy control strategy for an MMC controlled as a grid-forming unit under unbalanced conditions. Frequency-adaptivity in the detection of average energy signals is achieved with a SOGI-based frequency-adaptive notch filter (FA-NF). The performance of the FA-NF has been assessed in comparison to a moving average filter (MAF) or a fixed frequency notch filter (FF-NF) by numerical simulations and experimental results.

The SOGI-based FA-NF offers better dynamic performance than the MAF because it reduces the delay in the feedback loop, thereby increasing the stability region of the controllers. For the studied case, the phase margin of the open loop transfer function for the sum energy control is increased by 15.6°. Moreover, the FA-NF can effectively eliminate the selected frequency component with consistent performance independently from the operating frequency. However, the performance of control based on the FF-NF or the MAF will degrade when exposed to large deviations from the nominal grid frequency. The main comparative drawback is that the notch filter removes only the tuned harmonic components while the MAF attenuates all frequency components within the window width. Thus, the notch filter-based control scheme could allow for more background noise in the control loops.

The proposed scheme has been validated with VSM-based control but could be easily adapted to any other grid forming scheme relying on a power-balance-based synchronisation mechanism. Moreover, the operation has been verified for five different strategies for handling the negative sequence. In this perspective the FA-NF represents a versatile option to improve dynamic response and robustness, especially when the frequency is subjected to large variability as in cases of systems with weak frequency regulation (e.g. low inertia systems or islanded systems). Further work should be directed towards the integration of the proposed control strategy with methods for phase current limitation under severely unbalanced operating conditions.

REFERENCES

[1] S. C. Johnson, J. D. Rhodes, M. E. Webber, "Understanding the impact of non-synchronous wind and solar generation on grid stability and identifying mitigation pathways," in *Applied Energy*, Vol. 262, ID 114492, 11 pp., March 2020

[2] R. Rosso, X. Wang, M. Liserre, X. Lu, S. Engelken, "Grid-Forming Converters: Control Approaches, Grid-Synchronization, and Future Trends—A Review," in *IEEE Open Journal of Industry Applications*, Vol. 2, pp. 93-109, April 2021

[3] ENTSO-E Technical Group on High Penetration of Power Electronic Interfaced Power Sources, Tehcnial Report "High Penetration of Power Electronic Interfaced Power Sources and the Potential Contribution of Grid Forming Converters, 2020, available from: https://euagenda.eu/upload/publications/untitled-292051-ea.pdf

[4] M. A. Perez, S. Ceballos, G. Konstantinou, J. Pou and R. P. Aguilera, "Modular Multilevel Converters: Recent Achievements and Challenges," in *IEEE Open Journal of the Industrial Electronics Society*, Vol. 2, pp. 224-239, February 2021

[5] G. Li and J. Liang, "Modular Multilevel Converters: Recent Applications," in *IEEE Electrification Magazine*, Vol. 10, No. 3, pp. 85-92, September 2022

[6] E. Sánchez-Sánchez, E. Prieto-Araujo, O. Gomis-Bellmunt, "The Role of the Internal Energy in MMCs Operating in Grid-Forming Mode" in *IEEE Journal of Emerging and Selected Topics in Power Electronics*, Vol. 8, No. 2, pp. 949-962, June 2020

[7] E. Rokrok, T. Qoria, A. Bruyere, B. Francois, H. Zhang, M. Belhaouane, X. Guillaud "Impact of grid-forming control on the internal energy of a modular multilevel converter," *Proceedings of the 22nd European Conference on Power Electronics and Applications,* EPE'20 ECCE Europe, Lyon, France, 7-11 Sept. 2020, 10 pp.

[8] J. Arévalo-Soler, E. Sánchez-Sánchez, E. Prieto-Araujo, O. Gomis-Bellmunt, "Impact analysis of energy-based control structures for grid-forming and grid-following MMC on power system dynamics based on eigenproperties indices," in *Int. Journal of Electric Power and Energy Syst.*, Vol. 143, Article number 108369, 15 pp., December 2022

[9] C. Li, J. Xu, C. Zhao, "A Coherency-Based Equivalence Method for MMC Inverters Using Virtual Synchronous Generator Control, in *IEEE Trans. on Power Delivery*, Vol. 31, No. 3, pp. 1369-1378, June 2016

[10] C. Verdugo, J. I. Candela, P. Rodriguez, "Grid Support Functionalities based on Modular Multilevel Converters with Synchronous Power Control," in *Proceedings of the. 5th International Conference on Renewable Energy Research and Applications*, Birmingham, UK, 20-23 November 2016, pp. 572-577

[11] Z. Lv, Q.-C. Zhong, "Control of Modular Multilevel Converters as Virtual Synchronous Machines," in *Proceedings of the 2017 IEEE Power & Energy Society General Meeting*, Chicago, Illinois, USA, 16-20 July 2017, 5 pp.

[12] S. D'Arco, G. Guidi, J. A. Suul, "Operation of a Modular Multilevel Converter Controlled as a Virtual Synchronous Machine," in *Proceedings of the International Power Electronics Conference*, IPEC 2018 ECCE Asia, Niigata, Japan, 20-24 May 2018, 8 pp.

[13] D. Zhang, X. Li, D. Huang, Y. Chen, P. Li, L. Guoi, "Average Modeling and Stability Analysis of Virtual Synchronous Generator Controlled Modular Multilevel Converters," in *Proceedings of the 2018 International Conference on Power System Technology.*, POWERCON 2018, Guangzhou, China, 6-8 Nov. 2018, 8 pp.

[14] J. Li, G. Konstantinou, H. R. Wickramasinghe and J. Pou, "Operation and Control Methods of Modular Multilevel Converters in Unbalanced AC Grids: A Review," in *IEEE Journal of Emerging and Selected Topics in Power Electronics*, Vol. 7, No. 2, pp. 1258-1271, June 2019

[15] J. Freytes, J. Li, G. de Préville and M. Thouvenin, "Grid-Forming Control With Current Limitation for MMC Under Unbalanced Fault Ride-Through," *IEEE Transactions on Power Delivery*, Vol. 36, No. 3, pp. 1914-1916, June 2021

[16] J.-W. Moon, C.-S. Kim, J.-W. Park, D.-W. Kang and J.-M. Kim, "Circulating Current Control in MMC Under the Unbalanced Voltage," in *IEEE Trans. Power Del.*, vol. 28, no. 3, pp. 1952-1959, July 2013

[17] C. Hirsching, M. Goertz, S. Wenig, A. Bisseling, M. Suriyah and T. Leibfried, "On Fault-Ride-Through Performance in MMC-HVDC Applications Controlled as a Virtual Synchronous Machine," in *IEEE Trans. Energy Conv.*, Vol. 37, No. 4, pp. 2803-2812, December 2022

[18] E. B. Avdiaj, J. A. Suul, S. D'Arco, L. Piegari, "Adaptive Filtering for Energy Control of a Modular Multilevel Converter Operated as a Virtual Synchronous Machine Under Unbalanced Conditions," in *Proc. 16th Int. Conf. on Compatibility, Power Electron. and Power Eng.*, CPE-POWERENG, Birmingham, UK, 29th June – 1 July 2022, 8 pp.

[19] E. Avdiaj, J. Are Suul, S. D'Arco, L. Piegari, "A Current Controlled Virtual Synchronous Machine Adapted for Operation under Unbalanced Conditions," in *Proc. 9th Int. Conf. on Renewable Energy Research and Application*, ICRERA 2020, Glasgow, UK / Virtual Conference, 27-30 September 2020, pp. 263-270

[20] E. B. Avdiaj, S. D'Arco, L. Piegari, J. A. Suul, "Negative Sequence Control for Virtual Synchronous Machines Under Unbalanced Conditions," in *IEEE Journal of Emerging and Selected Topics in Power Electronics*, Vol. 10, No. 5, October 2022, pp. 5670-5685

[21] F. J. Rodríguez, E. Bueno, M. Aredes, L. G. B. Rolim, F. A. S. Neves, M. C. Cavalcanti, "Discrete-time implementation of second order generalized integrators for grid converters," in *Proceedings of the 34th Annual Conference of the IEEE Industrial Electronics Society*, IECON 2008, Orlando, Florida, USA, 10-13 November 2008, pp.176-181

[22] S. D'Arco, J. A. Suul, "Virtual Synchronous Machines – Classification of Implementations and Analysis of Equivalence to Droop Controllers for Microgrids," in *Proceedings of IEEE PES PowerTech 2013*, Grenoble, France, 16-20 June 2013, 7 pp.

[23] P. Rodríguez, R. Teodorescu, I. Candela, A. V. Timbus, M. Liserre, F. Blaabjerg, "New positive-sequence voltage detector for grid synchronization of power converters under faulty grid conditions," in *Proceedings of the 37th IEEE Power Electronics Specialists Conference*, PESC 2006, Jeju, South Korea, 18-22 June 2006, pp. 1-7

[24] O. Mo, S. D'Arco, J. A. Suul, "Evaluation of Virtual Synchronous Machines with Dynamic or Quasi-stationary Machine Models," in *IEEE Transactions on Industrial Electronics*, Vol. 64, No. 7, pp. 5952-5962, July 2017

[25] A. Antonopoulos, L. Ängquist, H.-P. Nee, "On dynamics and voltage control of the modular multilevel converter," in *Proceedings of the 13th European Conference on Power Electronics and Applications*, EPE'09, Barcelona, Spain, 8-10 September 2009, 10 pp.

[26] G. Bergna-Diaz, J. A. Suul, E. Berne, J.-C. Vannier, M. Molinas, "Optimal Shaping of the MMC Circulating Currents for Preventing AC-side Power Oscillations from Propagating into HVDC Grids" in *IEEE Journal of Emerging and Selected Topics in Power Electronics*, Vol. 7, No. 2, pp. 1015-1030, June 2019

[27] G. Guidi, S. D'Arco, K. Nishikawa, J. A. Suul, "Load Balancing of a Modular Multilevel Grid Interface Converter for Transformer-Less Large-Scale Wireless Electric Vehicle Charging Infrastructure," *IEEE Journal of Emerging and Selected Topics in Power Electronics*, Vol. 9, No, 4, pp. 4587-4605, Aug. 2021

[28] D. Soto-Sanchez, T. C. Green, "Control of a modular multilevel converter-based HVDC transmission system," in *Proceedings of the. 14th European Conference on Pow Electronics and. Applications*, EPE 2011, Birmingham, UK, 30 Aug– 1 Sept. 2011, 10 pp.

[29] A. E. Leon and S. J. Amodeo, "Energy Balancing Improvement of Modular Multilevel Converters Under Unbalanced Grid Conditions," in *IEEE Transactions on Power Electronics*, Vol. 32, No. 8, Aug. 2017, pp. 6628-6637

[30] S. Yang, J. Fang, Y. Tang, H. Qiu, C. Dong and P. Wang, "Modular Multilevel Converter Synthetic Inertia-Based Frequency Support for Medium-Voltage Microgrids," in *IEEE Transactions on Industrial Electronics*, Vol. 66, No. 11, pp. 8992-9002, November 2019

[31] R. O. de Sousa, A. F. Cupertino, J. V. Matos Farias, H. A. Pereira, "Modulation Strategy Impact on the Energy Storage Requirements of Modular Multilevel Converter-Based STATCOM," in Journal of Control Automation and Electrical Systems, early access, April 2023

[32] S. Golestan, M. Ramezani, J. M. Guerrero, F. D. Freijedo, M. Monfared, "Moving Average Filter Based Phase-Locked Loops:

Performance Analysis and Design Guidelines," in *IEEE Transactions on Power Electronics*, Vol. 29, No. 6, pp.2750-2736, June 2014

[33] G. Bergna, J. A. Suul, A. Garcés, E. Berne, P. Egrot, A. Arzandé, J.-C. Vannier, M. Molinas, "Improving the Dynamics of Lagrange-based MMC Controllers by means of Adaptive Filters for Single-Phase Voltage, Power and Energy Estimation," in *Proceedings of the 39th Annual Conference of the IEEE Industrial Electronivs Society*, IECON, Vienna, Austria, 10-13 Nov. 2013, pp. 6237-6242

[34] J. Fang, H. Li, Y. Tang and F. Blaabjerg, "On the Inertia of Future More-Electronics Power Systems," in *IEEE Journal of Emerging and Selected Topics in Power Electronics*, Vol. 7, No. 4, pp. 2130-2146, December 2019

[35] P. Rodriguez, A. Luna, R. S. Muñoz-Aguilar, I. Etxeberria-Otadui, R. Teodorescu, F. Blaabjerg, "A Stationary Reference Frame Grid Synchronization System for Three-Phase Grid-Connected Power Converters Under Adverse Grid Conditions", *IEEE Transactions on Power Electronics*, Vol. 27, No. 1, pp. 99-112, January 2012

[36] J. Peralta, H. Saad, S. Dennetiere, J. Mahseredjian and S. Nguefeu, "Detailed and Averaged Models for a 401-Level MMC–HVDC System," in IEEE Trans. on Power Del., vol. 27, no. 3, pp. 1501-1508, July 2012

[37] K. Ljøkelsøy, G. Guidi, "Development of a scale model of a Modular Multilevel Converters," in *Proc. 14th Deep Sea Offshore Wind R&D Conference*, EERA DeepWind'2017, 18-20 January 2017, Trondheim Norway, Energy Procedia, Vol. 137, October 2017, pp. 505-513

[38] G. Bergna J. A. Suul, S. D'Arco, "State-Space Modeling of Modular Multilevel Converters for Constant Variables in Steady-State," in *Proceedings of the 17th IEEE Workshop on Control and Modeling for Power Electronics*, COMPEL 2016, Trondheim, Norway, 27-30 June 2016, 9 pp.

Eros B. Avdiaj was born in Tirana, Albania, in 1995. He received the M. Sc (cum laude) degree in electrical engineering from Politecnico di Milano, Italy, in 2020. He is currently working toward a Ph.D. degree in harmonic and stability assessment of future grid-forming converters at KU Leuven/ EnergyVille, Belgium.

In 2020 he performed his master's thesis research during an internship of ten months at SINTEF Energy Research, Trondheim, Norway, on the operation of grid-forming HVDC converters under unbalanced conditions. In March 2020, Mr. Avdiaj was part of the winning team in the ABB challenge in EV-charging. His research interest includes future power system dynamics, control, and modelling of power electronic converters.

Salvatore D'Arco received the M.Sc. and Ph.D. degrees in electrical engineering from the University of Naples "Federico II," Naples, Italy, in 2002 and 2005, respectively.

From 2006 to 2007, he was a postdoctoral researcher at the University of South Carolina, Columbia, SC, USA. In 2008, he joined ASML, Veldhoven, the Netherlands, as a Power Electronics Designer, where he worked until 2010. From 2010 to 2012, he was a postdoctoral researcher in the Department of Electric Power Engineering at the Norwegian University of Science and Technology (NTNU), Trondheim, Norway. In 2012, he joined SINTEF Energy Research where he currently works as a Chief Research Scientist. He is the author of more than 100 scientific papers and is the holder of one patent. His main research activities are related to control and analysis of power-electronic conversion systems for power system applications, including real-time simulation and rapid prototyping of converter control systems.

Luigi Piegari (M'04-SM'13) was born in Naples, Italy, on April 2, 1975. He received the M.S. (cum laude) and Ph.D degrees in Electrical Engineering from the University of Naples Federico II, Italy, in 1999 and 2003, respectively.

He was, from 2003 to 2008, a Postdoctoral Research Fellow in the Department of Electrical Engineering, University of Naples Federico II, Italy. From 2009 to 2012, he was assistant professor at Department of Electrical Engineering of the Polytechnic University of Milan. He is currently associate professor of Electrical Machines and Drives at the Department of Electronics, Information and Bioengineering of the Polytechnic University of Milan. He is the author of more than 130 scientific papers published in international journals and conference proceedings. His research interests include storage devices modelling, wind and photovoltaic generation, modelling and control of multilevel converters and DC distribution grids.

Prof. Piegari is a member of the IEEE Industrial Electronics Society, of the IEEE Power Electronics Society and of AEIT. He is associate editor of the IEEE Journal of Emerging and selected topics in industrial electronics and technical program chair of the International Conference on Clean Electrical Power.

Jon Are Suul (M'11) received the M.Sc. degree in energy and environmental engineering and the Ph.D. degree in electric power engineering from the Norwegian University of Science and Technology (NTNU), Trondheim, Norway, in 2006 and 2012, respectively.

From 2006 to 2007, he was with SINTEF Energy Research, Trondheim, where he was working with simulation of power electronic converters and marine propulsion systems until starting his Ph.D. studies. Since 2012, he has been a Research Scientist with SINTEF Energy Research, first in a part-time position while working as a part-time Postdoctoral Researcher with the Department of Electric Power Engineering of NTNU until 2016. Since August 2017, he has been an Adjunct Associate Professor with the Department of Engineering Cybernetics, NTNU. His research interests are mainly related to modelling, analysis, and control of power electronic converters in power systems, renewable energy applications, and electrification of transport.

Dr. Suul is an Editor of the IEEE Journal of Emerging and Selected Topics in Power Electronics, and an Associate Editor of the IEEE Journal of Emerging and Selected topics in industrial electronics.